Supplement of Atmos. Chem. Phys., 14, 12631–12649, 2014
http://www.atmos-chem-phys.net/14/12631/2014/
doi:10.5194/acp-14-12631-2014-supplement

Atmospheric Chemistry and Physics Open Access

Supplement of

Aerosol–computational fluid dynamics modeling of ultrafine and black carbon particle emission, dilution, and growth near roadways

L. Huang et al.

Correspondence to: L. Huang (li.huang@utoronto.ca)

Supplement of Atmos. Chem. Phys., 14, 12631–12649, 2014
http://www.atmos-chem-phys.net/14/12631/2014/
doi:10.5194/acp-14-12631-2014-supplement

Atmospheric Chemistry and Physics Open Access

Supplement of

Aerosol–computational fluid dynamics modeling of ultrafine and black carbon particle emission, dilution, and growth near roadways

L. Huang et al.

Correspondence to: L. Huang (li.huang@utoronto.ca)

Supplement of Atmos. Chem. Phys., 14, 12631–12649, 2014
http://www.atmos-chem-phys.net/14/12631/2014/
doi:10.5194/acp-14-12631-2014-supplement

Atmospheric Chemistry and Physics Open Access

Supplement of

Aerosol–computational fluid dynamics modeling of ultrafine and black carbon particle emission, dilution, and growth near roadways

L. Huang et al.

Correspondence to: L. Huang (li.huang@utoronto.ca)

Supplement Information

S1 Site map

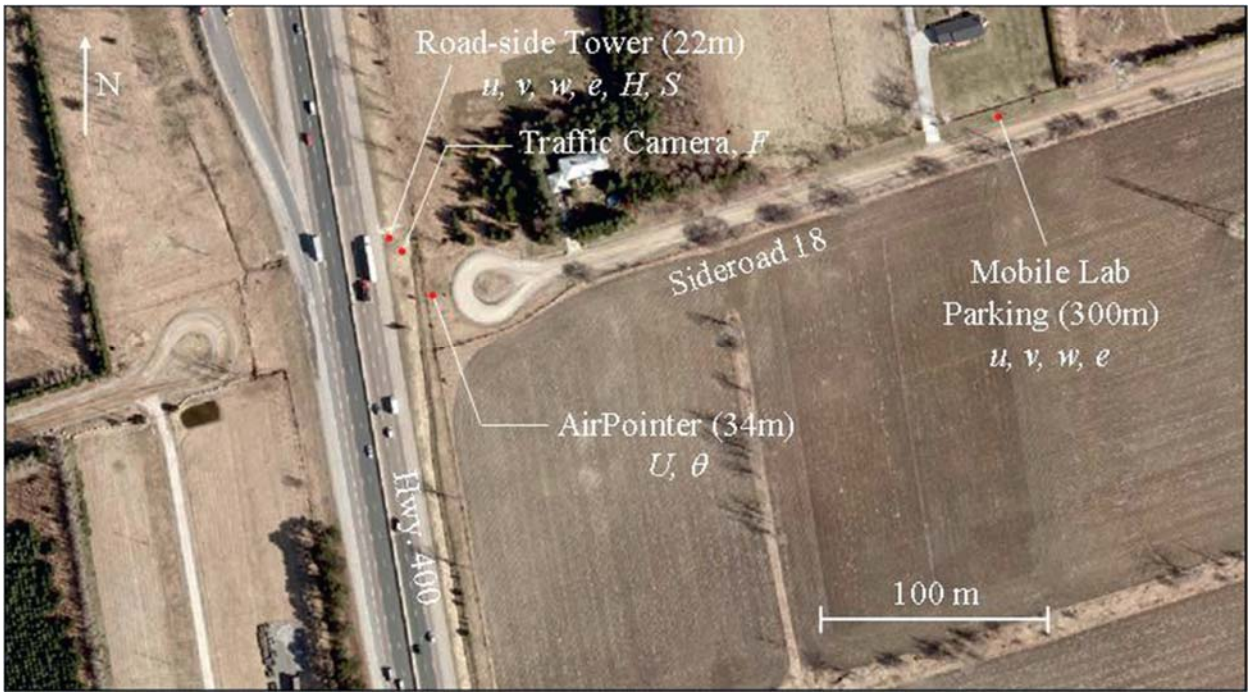

Fig. S1. FEVER study site map (originally from Fig. 2 in (Gordon et al., 2012b)).

S2 Grid cell size validation

For the verification of the grid cell size used in the near-road dispersion simulations, we carry out a series of simulations using three grid cell sizes: coarse, current, and fine grids. The current grid cell size is documented in Section 3.2. We initially start from a coarse grid, which has approximately half the number of grid cells in the x, y, and z coordinates of the current grid. To generate the current grid for the whole domain, 2 times the number of grid cells in all three coordinates is used, and the fine grid has doubled number of grid cells of the current grid. Therefore, the total grid cell numbers of the whole domain increases by a factor of approximately 8 from the coarse grid to the fine grid. For the base case scenario with all three grid configurations, the simulated turbulence (TKE and dissipation rate) and pollutant concentrations at Site B (located 34 m east of the highway centre) are summarized in Table S1. The results show that for both turbulence quantities and pollutant concentrations, the improvement of the grid cell size refinement over the current grid configuration is negligible (less than 3%). However, the grid coarsening would result in significantly overestimated turbulence, therefore, underestimated pollutant concentrations at Site B.

Table S1. Grid cell size validation results for near-road dispersion simulations, measured by changes in percentage with respect to the current grid cell size configuration results.

	Coarse grid	**Current grid**	**Fine grid**
TKE (k)	26%	0%	1%
Dissipation rate (ε)	55%	0%	3%
CO_2	-1%	0%	0%
Black carbon (BC)	-48%	0%	3%
Particle number (N)	-61%	0%	1%

For the verification of the grid cell size used in on-road TKE simulations, a similar series of simulations are conducted for Sedan and SUV travelling at V=20 m/s. The computational domain for on-road TKE simulations is 20 m (lateral) ×350 m (streamwise) ×15 m (vertical), which is determined based on available measurements of TKE and in compliance with (Franke, 2007). For the current grid used in our work, there are about 6×10^6 unstructured hexahedral cells. Since we focus on on-road turbulence, the grid validation results are only presented for TKE (k) in Table S2. The results suggest simulations are grid independent for the current grid configurations.

Table S2. Grid cell size validation results of on-road TKE simulations for Sedan and SUV, measured by TKE changes in percentage with respect to the current grid cell size configuration results.

Vehicle type	**Coarse grid**	**Current grid**	**Fine grid**
Sedan	20%	0%	1%
SUV	25%	0%	1%

S3 Assumption of stationary conditions

We assume that stationary boundary condition is valid for the current work based on the following reasons. Firstly, the meteorological conditions remained relatively unchanged for the periods of investigation (i.e. 05:00-08:00 a.m. of 14 and 15 September 2010). The most relevant meteorological conditions to the near road dispersion of pollutants include the wind speed and direction and the atmospheric stability condition. The FEVER field study was designed to monitor pollutant gradients perpendicular to Hwy-400 under predominant wind from the west. Following the previous analysis (Gordon et al., 2012a), the measured turbulence and pollutant concentrations are filtered for winds within 45° of the highway normal, which results in removing less than 5% of the data. Previous results on the variations in the measured wind speed and atmospheric stability condition show persistent diurnal patterns (Fig. 2 in (Gordon et al., 2012a)). The case study period of 05:00-08:00 a.m. of 14 and 15 September 2010 is specifically chosen due to this ideal perpendicular wind condition (within 5° on average). Secondly, both the traffic volume and the travelling speed show persistent diurnal patterns and stability within the period of chosen (Fig. 2 in (Gordon et al., 2012a)). Finally, the residence time (of about 400 s) estimated based on 3-m wind speed measured on site is much less than the averaging period of 1 hour for the half traffic case (05:00-06:00 a.m.) and 2 hours for the base case (06:00-08:00 a.m.). Therefore, the assumption of stationary conditions is considered valid in our case study.

S4 Modelling the transition from ABL to vehicle wake region

In this work, we did employ a different approach for the vehicle wake regions, as proposed by Parente et al. (2011). This approach allows a gradual transition in Sε and Cμ from the fully developed ABL (dominated by ABLT) to the wake region (dominated by VIT). Following the above-mentioned article, a coefficient (δ) was defined in Eq. S1 as the deviation of the actual local velocity profile with respect to the inlet logarithmic profile. This coefficient was used in a quadratic transition function (Eq. S2) to blend Sε and Cμ to account for the transition from fully developed ABL to the wake region. In the following equations, u stands for local velocity profile; $u_{\log,ABL}$ stands for fully developed inlet ABL velocity profile; ϕ is either Sε or Cμ; the subscript std refers to the standard k-ε model values (Sε=0 and Cμ=0.09).

$$\delta = \min\left[\frac{u - u_{\log,ABL}}{u_{\log,ABL}}, 1\right] \quad \text{(Eq. S1)}$$

$$\phi = \phi_{std} + (1-\delta^2)(\phi_{ABL} - \phi_{std}) \quad \text{(Eq. S2)}$$

Reference:

Franke, J.: Best practice guideline for the CFD simulation of flows in the urban environment, Meteorological Inst., 2007.

Gordon, M., Staebler, R. M., Liggio, J., Li, S.-M., Wentzell, J., Lu, G., Lee, P., and Brook, J. R.: Measured and modeled variation in pollutant concentration near roadways, Atmos. Environ., 57, 10.1016/j.atmosenv.2012.04.022, 2012a.

Gordon, M., Staebler, R. M., Liggio, J., Makar, P., Li, S.-M., Wentzell, J., Lu, G., Lee, P., and Brook, J. R.: Measurements of Enhanced Turbulent Mixing near Highways, Journal of Applied Meteorology and Climatology, 51, 10.1175/jamc-d-11-0190.1, 2012b.

Parente, A., Gorle, C., van Beeck, J., and Benocci, C.: A Comprehensive Modelling Approach for the Neutral Atmospheric Boundary Layer: Consistent Inflow Conditions, Wall Function and Turbulence Model, Bound.-Layer Meteor., 140, 411-428, 10.1007/s10546-011-9621-5, 2011.